CMS Physics Analysis Summary

Contact: cms-pag-conveners-susy@cern.ch 2012/11/15

Search for direct top squark pair production in events with a single isolated lepton, jets and missing transverse energy at $\sqrt{s} = 8$ TeV

The CMS Collaboration

Abstract

This note presents a search for top squark pair production in events with a single isolated electron or muon, jets, and large missing transverse energy. At least one of the jets is required to be identified as originating from a b-quark and events are required to have large transverse mass. The data sample used corresponds to an integrated luminosity of 9.7 fb^{-1} of pp collisions, collected in 2012 by the CMS experiment at the LHC, at a centre-of-mass energy of 8 TeV. No significant excess in data is observed above the expected standard model backgrounds. The results are interpreted in the context of models of top squark pair production where the top squarks decay either to a top quark and a neutralino or to a bottom quark and a chargino. Depending on the decay mode, the results probe top squarks with masses in the range of $160 - 430$ GeV.

1 Introduction

The standard model (SM) has been incredibly successful at describing the majority of particle physics phenomena. However, it suffers from such shortcomings as the hierarchy problem, where fine-tuned cancellations of large quantum corrections are required in order for the Higgs boson to have a mass of order 100 GeV, at the electroweak symmetry breaking scale. Supersymmetry (SUSY) is a popular extension to the SM which postulates that for each SM particle there exists a superpartner with exactly the same quantum numbers, differing by one half unit of spin. SUSY provides a natural solution to the hierarchy problem through the exact cancellations of the quadratic divergences of the top quark and scalar top squark loops. In addition, it provides a connection to the cosmological sector, with the lightest supersymmetric particle (LSP), if neutral and stable, serving as a dark matter candidate.

This note documents a search for the pair production of top squarks, in a dataset corresponding to an integrated luminosity of 9.7 fb^{-1} collected at $\sqrt{s} = 8$ TeV by the Compact Muon Solenoid (CMS) experiment at the LHC during 2012. This search is motivated by the fact that relatively light top squarks are necessary if SUSY is to be the "natural", i.e., not fine-tuned, solution to the gauge hierarchy problem [1–5]. These constraints are especially relevant given the recent discovery of a particle that closely resembles the Higgs boson, with a mass of 125 GeV [6]. Searches for top squark pair production have been performed by the ATLAS collaboration at the LHC in several final states [7–11], and by the CDF [12] and D0 [13] collaborations at the Tevatron.

The search presented focuses on two decay modes of the top squark ($\tilde{t}$): $\tilde{t} \to t\tilde{\chi}_1^0 \to b\mathrm{W}\tilde{\chi}_1^0$ and $\tilde{t} \to b\tilde{\chi}_1^+ \to b\mathrm{W}\tilde{\chi}_1^0$, which are expected to have large branching fractions if kinematically accessible. Here the neutralinos ($\tilde{\chi}^0$) and charginos ($\tilde{\chi}^+$) are the mass eigenstates formed by the linear combination of the gauginos and higgsinos, fermionic superpartners of the gauge and Higgs bosons. The charginos are unstable and can subsequently decay into neutralinos and W bosons, leading to the following processes of interest: $pp \to \tilde{t}\bar{t}^* \to t\bar{t}\tilde{\chi}_1^0\tilde{\chi}_1^0 \to b\bar{b}\mathrm{W}^+\mathrm{W}^-\tilde{\chi}_1^0\tilde{\chi}_1^0$ and $pp \to \tilde{t}\bar{t}^* \to b\bar{b}\tilde{\chi}_1^+\tilde{\chi}_1^- \to b\bar{b}\mathrm{W}^+\mathrm{W}^-\tilde{\chi}_1^0\tilde{\chi}_1^0$, as displayed in Fig. 1. The lightest neutralino $\tilde{\chi}_1^0$ is often considered to be the stable LSP, which escapes without detection and results in large missing transverse energy ($E_\mathrm{T}^\mathrm{miss}$).

The signature of the signal process includes high transverse momentum jets, including two b-jets, and $E_\mathrm{T}^\mathrm{miss}$. Requiring exactly one isolated, high p_T electron or muon suppresses many of the dominant backgrounds present in the all-hadronic channel. The largest backgrounds in the single lepton topology are semi-leptonic decays of $\mathrm{t\bar{t}}$ and W+jets. These backgrounds

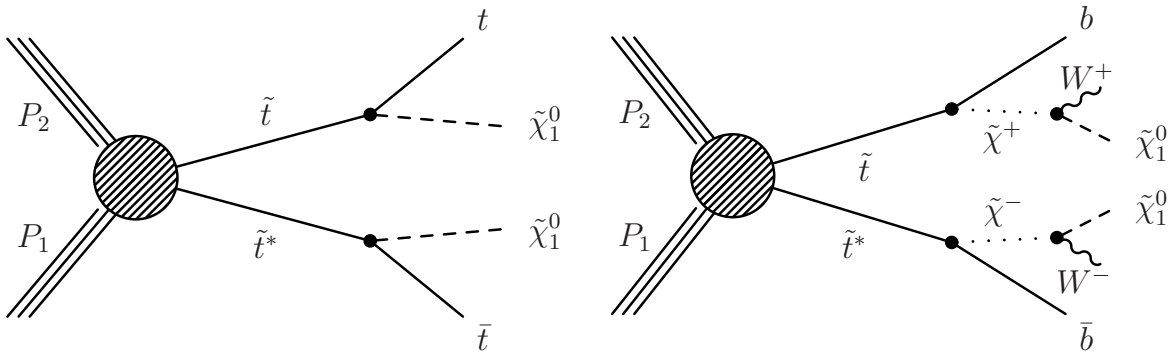

Figure 1: Diagram for top squark pair production for the $\tilde{t} \to t\tilde{\chi}_1^0 \to b\mathrm{W}\tilde{\chi}_1^0$ decay mode (left) and the $\tilde{t} \to b\tilde{\chi}_1^+ \to b\mathrm{W}\tilde{\chi}_1^0$ decay mode (right).

contain a single leptonically-decaying W boson, and the transverse mass (M_{T}) of the lepton-neutrino system has a kinematic endpoint requiring $M_{\mathrm{T}} < M_W$. For the signal, the presence of additional LSP's in the final state allows M_{T} to exceed M_W. Hence we search for an excess of events with large M_{T}. The dominant background in this kinematic region is dilepton $\mathrm{t\bar{t}}$ where one of the leptons is not identified, since the presence of the additional neutrino from the second leptonically-decaying W boson allows M_{T} to exceed M_W.

The expected top squark pair production cross section varies between O(10) pb for $m_{\tilde{t}} = 200$ GeV and O(0.01) pb for $m_{\tilde{t}} = 500$ GeV. The critical challenge of this analysis is that the kinematic distributions, in particular M_{T}, are very similar to SM $\mathrm{t\bar{t}}$ production, even though the production cross section for light top squarks ($m_{\tilde{t}} \approx m_t$) is reasonably large. In this regime it becomes very difficult to distinguish the signal and background. For large top squark masses the kinematic distributions for signal events differ from those from SM $\mathrm{t\bar{t}}$ production, but the cross section decreases rapidly, reducing the signal-to-background ratio.

2 CMS detector

The central feature of the CMS apparatus is a superconducting solenoid, 13 m in length and 6 m in diameter, which provides an axial magnetic field of 3.8 T. Within the field volume are several particle detection systems. Charged particle trajectories are measured by silicon pixel and silicon strip trackers, covering $0 \leq \phi < 2\pi$ in azimuth and $|\eta| < 2.5$ in pseudorapidity, where $\eta = -\ln[\tan(\theta/2)]$ and θ is the polar angle of the trajectory of the particle with respect to the counterclockwise proton beam direction. A lead tungstate crystal electromagnetic calorimeter and a brass/scintillator hadron calorimeter surround the tracking volume, providing energy measurements of electrons and hadronic jets. Muons are identified and measured in gas-ionization detectors embedded in the steel flux return yoke of the solenoid. The CMS detector is nearly hermetic, allowing momentum balance measurements in the plane transverse to the beam direction. A two-tier trigger system selects pp collision events of interest for use in physics analyses. A more detailed description of the CMS detector can be found elsewhere [14].

3 Event samples, reconstruction, and selection

The data used for this measurement were collected using single high-p_{T} isolated electron and muon triggers with p_{T} thresholds of 27 GeV and 24 GeV, respectively. Additionally, data collected using high-p_{T} double-lepton triggers (ee, eμ, or $\mu\mu$, with p_{T} thresholds of 17 GeV and 8 GeV on the two leptons) are used in the dilepton control region used to verify the $\mathrm{t\bar{t}}$ background modeling.

3.1 Pre-selection

Muon candidates are reconstructed using an algorithm that performs a global fit requiring consistent hit patterns in the tracker and the muon system (globally fitted muons) [15]. Electron candidates are reconstructed starting from a cluster of energy deposits in the electromagnetic calorimeter. The cluster is then matched to signals in the silicon tracker. A selection using electron identification variables based on shower shape and track-cluster matching is applied to the reconstructed candidates [16]. Electron candidates within $\Delta R \equiv \sqrt{(\Delta\eta)^2 + (\Delta\phi)^2} < 0.1$ from a selected muon are rejected to remove candidates due to muon bremsstrahlung and final-state radiation. Both electrons and muons are required to be isolated from other activity in the event. This is achieved by imposing a maximum allowed value of either 0.15 on the ratio of the scalar sum of track transverse momenta and calorimeter transverse energy deposits

within a cone of $\Delta R < 0.3$ around the lepton candidate direction at the origin (the transverse momentum of the candidate is excluded), to the transverse momentum of the candidate, or 5 GeV, whichever is smaller. The expected contribution from pile-up is subtracted from the lepton isolation sum. Electrons have additional requirements imposed on them to remove mismeasured and fake candidates. The ratio of the electron energy to the momentum of the seeding track is required to be smaller than 4. We also require that the difference between the electron momentum as reconstructed by the default algorithm and the particle-flow algorithm [17] does not exceed 10 GeV.

At the pre-selection stage, we require events to have an isolated lepton with transverse momentum $p_{\mathrm{T}} > 30\,\mathrm{GeV}/c$. The electrons are required to be in the barrel region of the electromagnetic calorimeter $|\eta| < 1.4442$, while allowed pseudorapidity coverage for the muons extends to $|\eta| < 2.1$. In addition to the lepton, we require events to have at least four jets and moderate missing transverse energy. The jets and the missing transverse energy $E_{\mathrm{T}}^{\mathrm{miss}}$ are reconstructed with a particle-flow technique. The anti-k_{T} clustering algorithm [18] with a distance parameter of 0.5 is used for jet clustering. At least four jets with $p_{\mathrm{T}} > 30\,\mathrm{GeV}/c$ and $|\eta| < 2.5$, separated by $\Delta R > 0.4$ from leptons passing the analysis selection, are required in each event. At least one of these jets is required to be consistent with coming from the decay of heavy flavor hadrons, as identified by the Combined Secondary Vertex Medium Point (CSVM) b-tagging algorithm [19], which is based on the reconstruction of a secondary vertex. The $E_{\mathrm{T}}^{\mathrm{miss}}$ in the event is required to exceed 50 GeV.

Finally, in order to reduce background from dilepton $\mathrm{t\bar{t}}$, we reject events that contain isolated tracks with transverse momentum greater than 10 GeV, in addition to the selected lepton.

With the steadily increasing LHC instantaneous luminosity, the mean number of interactions in a single bunch crossing also increased over the course of data taking. In the following, the yields of simulated events are reweighted to reproduce the distribution of reconstructed vertices observed in data. The efficiencies of the triggers are measured using studies of $\mathrm{Z}\to\ell\ell$ ($\ell = \mathrm{e}, \mu$) events in data, and these efficiencies are applied to the yields predicted from simulation.

3.2 Signal Regions

To enhance sensitivity to top squark pair production, additional requirements are imposed on the events passing the pre-selection. Because the kinematics of signal events change as a function of the top squark and LSP masses, several signal regions (SR's) are introduced. The additional requirements, placed on $E_{\mathrm{T}}^{\mathrm{miss}}$ and M_{T}, are summarized in Table 1. The large M_{T} requirement strongly suppresses the background from W+jets and semi-leptonic $\mathrm{t\bar{t}}$, and we explore a range of $E_{\mathrm{T}}^{\mathrm{miss}}$ requirements to optimize the sensitivity over a range of values of the mass difference between the top squark and the LSP, $m_{\tilde{t}} - m_{\mathrm{LSP}}$. For the loosest signal region (SRA), for the $\tilde{t} \to t\tilde{\chi}_1^0$ and $\tilde{t} \to b\tilde{\chi}_1^{\pm}$ (with $m_{\tilde{\chi}_1^{\pm}} = 0.75 m_{\tilde{t}} + 0.25 m_{\tilde{\chi}_1^0}$) scenarios, the signal efficiency times acceptance varies from approximately 5% to 1% as the mass difference $\Delta m = m_{\tilde{t}} - m_{\tilde{\chi}_1^0}$ varies from 600 to 200 GeV. For the tightest signal region (SRG), the corresponding efficiencies vary from 1% to 0.1% as Δm varies from 600 to 400 GeV. Details of the signal modeling are presented in Section 9.

4 Background and Signal Modeling

In this Section we describe the Monte Carlo (MC) modeling of signal and backgrounds. We also present a general overview of the background estimation strategy, followed by further details

Signal Region	Minimum M_{T} [GeV]	Minimum $E_{\mathrm{T}}^{\mathrm{miss}}$ [GeV]
SRA	150	100
SRB	120	150
SRC	120	200
SRD	120	250
SRE	120	300
SRF	120	350
SRG	120	400

Table 1: Signal region definitions based on M_{T} and $E_{\mathrm{T}}^{\mathrm{miss}}$ requirements. These requirements are applied in addition to the baseline single lepton selection.

in Sec. 6.

The background is divided into four categories, which are each estimated separately. The largest background contribution is $\mathrm{t\bar{t}}$ production in which both W bosons decay leptonically ($\mathrm{t\bar{t}} \to \ell\ell$), but one of the leptons is not selected. This process contributes approximately (60–70)% of the total background in the various signal regions. The second largest background consists of $\mathrm{t\bar{t}}$ production in which one W boson decays leptonically and the other hadronically ($\mathrm{t\bar{t}} \to \ell + \text{jets}$), as well as single top production in the s-channel and t-channel modes. These are collectively referred to as "single lepton top" processes, and they contribute approximately (15–30)% of the total background. The third largest background consists of a variety of SM processes with small cross section, including $\mathrm{t\bar{t}}$ produced in association with a vector boson ($\mathrm{t\bar{t}W}$, $\mathrm{t\bar{t}Z}$, $\mathrm{t\bar{t}}\gamma$), processes with two (WW, WZ, ZZ) and three (WWW, WWZ, WZZ, ZZZ) electroweak vector bosons, and single top production in the tW-channel mode. These procesess are collectively referred to as the "rare" processes and contribute approximately (5–20)% of the total background. The production of Z bosons in association with jets from initial state radition (ISR) (Z+jets) is also included in this category; although the cross section for this process is quite large this background is strongly suppressed by the jets and $E_{\mathrm{T}}^{\mathrm{miss}}$ requirements, and the contribution in the signal regions is very small. The fourth and final background contribution is from the production of W bosons in association with jets from ISR (W+jets), contributing approximately (3–7)% of the total background.

Backgrounds are estimated using samples simulated with MC techniques. These samples are generated using the PYTHIA 6.4.22 [20], MADGRAPH 4.4.12 [21], or POWHEG [22] MC event generators using the CTEQ6.6 parton density functions [23] and are normalized to cross sections calculated at next-to-leading order (NLO). The nominal $\mathrm{t\bar{t}}$ sample is generated with POWHEG, but we verify that the background predictions do not depend significantly on the choice of MC generator or on the values of the generator parameters (Q^2 scale, matching scale, and top mass). Signal events are generated with PYTHIA 6.4.22. They are normalized to cross sections calculated at NLO in the strong coupling constant, including the resummation of soft gluon emission at next-to-leading-logarithmic accuracy (NLO+NLL) [24].

In the MC simulation of both signal and backgrounds, multiple proton-proton interactions are simulated by PYTHIA and superimposed on the hard collision, and the MC samples are reweighted to describe the distribution of reconstructed primary vertices in data. Standard Model processes are simulated using a GEANT4-based model [25] of the CMS detector; the simulation of new physics signals is performed using the CMS fast simulation package [26]. Events are finally reconstructed and analyzed with the same software used to process collision data.

A correction for possible mismodeling of the jet multiplicity in dilepton $t\bar{t}$ events ($t\bar{t} \to \ell\ell$) is performed in Sec. 5. Validation of the background modeling in the Monte Carlo in dedicated control regions is described in Section 6. These control regions are used to extract data/MC scale factors (where necessary) and corresponding systematic uncertainties.

Evaluation of the dominant backgrounds is based on the extrapolation from the observed number of events in the peak of the M_{T} distribution into the signal regions. First, to obtain the correct normalization, MC predictions for $t\bar{t}$ and W+jets are scaled to the data in the M_{T} peak region defined by $50 < M_T < 80$ GeV. This normalization is performed in two steps, in order to correct for possible MC mismodeling of the isolated track misidentification rate in the single lepton top and W+jets backgrounds. First, the $t\bar{t}$ and W+jets samples are normalized to data in the M_{T} peak region, after imposing all requirements except for the rejection of events with an isolated track. Second, the isolated track veto is imposed and a second scaling factor is applied to the single lepton backgrounds only (single lepton top and W+jets backgrounds) such that the total MC yield matches the data in the M_{T} peak region. This procedure corrects for potential differences in the isolated track misidentification rate in the data vs. MC, and relies on the fact that the efficiency to identify genuine isolated leptons is well-modeled in MC, which is verified using studies of $Z \to \ell\ell$ in data and MC.

The background predictions are then extrapolated into the M_{T} tail, using the "tail-to-peak ratio" (R) of the number of events with M_{T} satisfying the signal region requirement to the number of events in the M_{T} peak region. This ratio is larger for the W+jets background than for the single lepton top background. This is due to a significant contribution of very off-shell W bosons to the tail of the M_{T} distribution in W+jets events, which is not present for the single lepton top background since the W mass cannot exceed the difference between the top and bottom quark masses, $m_t - m_b$. Therefore, the tail-to-peak ratio for each of the signal regions is evaluated separately (from simulation) for the single lepton top and W+jets backgrounds. Data control samples are then used to extract data/MC scale factors and corresponding uncertainties for these tail-to-peak ratios. For W+jets events this is done in a sample defined by rejecting events with jets identified as originating from a b-quark. The tail-to-peak ratio for top events is validated in a similar fashion in a $Z \to \ell\ell$ sample with one lepton added to the $E_{\mathrm{T}}^{\mathrm{miss}}$ calculation. This sample is well suited to testing the jet resolution effects on the M_T tail, since off-shell W/Z effects are eliminated by the Z-mass requirement.

Background contributions from the processes referred to above as "rare" are taken directly from Monte Carlo and normalized to the corresponding NLO cross sections. The QCD contribution to the background is negligible in the signal regions due to the requirement of a high p_{T} isolated lepton, large M_{T} and $E_{\mathrm{T}}^{\mathrm{miss}}$, and the presence of a b-tagged jet.

5 Correction for Jet Multiplicity in $t\bar{t} \to \ell\ell$ Events

In this section, we derive correction factors for possible mismodeling of the jet multiplicity (N_{jets}) in $t\bar{t} \to \ell\ell$ events. This is required because $t\bar{t} \to \ell\ell$ events have only two jets from top decay, and additional jets from initial state or final state radition (ISR/FSR) are not necessarily well-modeled in simulation. A data control sample dominated by $t\bar{t} \to \ell\ell$ is defined by requiring the presence of exactly two opposite-sign selected leptons (electrons or muons) in events satisfying dilepton triggers. To suppress the Z+jets background, same-flavor (ee or $\mu\mu$) events with invariant mass in the range $76 < m_{\ell\ell} < 106$ GeV are rejected, we require the presence of at least one b-tagged jet, and impose minimum requirements on $E_{\mathrm{T}}^{\mathrm{miss}}$. We then compare the N_{jets} distribution in data vs. MC, as displayed in Fig. 2. This comparison is used to extract correction factors which are applied to MC $t\bar{t} \to \ell\ell$ events; however, since we observe reason-

able agreement between data and MC these correction factors are close to 1. The comparison between the data yields and MC predictions for the bin with exactly three jets is used to extract a correction factor for $t\bar{t} \to \ell\ell$ events with one additional jet from ISR/FSR and one additional jet from the decay of a lepton (corresponding to approximately 25% of the $t\bar{t} \to \ell\ell$ sample satisfying the signal region selection). The resulting correction is $K_3 = 1.01 \pm 0.03$, where the uncertainty includes the statistical uncertainty in the data and MC. The comparison between the data yields and MC predictions for the bin with four or more jets is used to extract a correction factor for $t\bar{t} \to \ell\ell$ events with at least two additional jets from ISR/FSR (corresponding to approximately 75% of the $t\bar{t} \to \ell\ell$ sample satisfying the signal region selection). The resulting correction is $K_4 = 0.93 \pm 0.04$, where the uncertainty includes the statistical uncertainty in the data and MC. The correction factors extracted by this procedure do not depend significantly on the choice of $E_{\mathrm{T}}^{\mathrm{miss}}$ requirement. These correction factors are applied to the MC $t\bar{t} \to \ell\ell$ events, and the above uncertainties on the K_3 and K_4 correction factors are propagated to the $t\bar{t} \to \ell\ell$ background prediction.

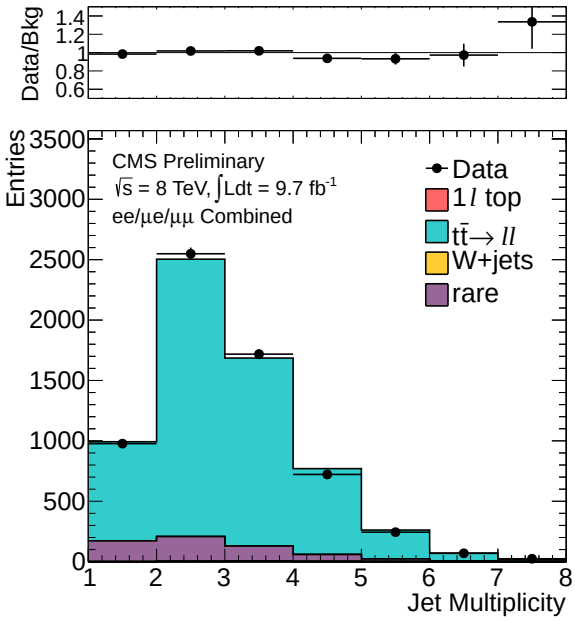

Figure 2: Comparison of the N_{jets} distributions in data vs. MC for the sample dominated by $t\bar{t} \to \ell\ell$, discussed in Sec. 5.

6 Control Region Studies

To validate the background predictions in the signal region, we define a set of control regions (CR) that are used to test the background estimation procedure and derive the systematic uncertainties on specific contributions. The CRs are chosen to have similar kinematics to the SRs, but have different requirements that are designed to enhance the contribution of a specific SM background.

The two selection requirements that are varied are the number of b-tags in the event and the number of leptons. The four CRs used in the analysis, labeled CR1-CR5 (CR3 is not used), are indicated, along with the signal region in Table 2. The dominant $t\bar{t} \to \ell\ell$ background is validated in two control regions, one with exactly two selected leptons (CR4) and one with

Selection Criteria	exactly 1 lepton	exactly 2 leptons	1 lepton + isolated track
0 b-tags	CR1) W+Jets dominated: Validate W+Jets M_{T} tail	CR2) apply Z-mass constraint $\rightarrow$ Z+Jets dominated: Validate $\mathrm{t\bar{t}} \rightarrow \ell +$ jets M_{T} tail comparing data vs. MC "pseudo-M_{T}"	CR3) not used
$\geq$ 1 b-tags	SIGNAL REGION	CR4) Apply Z-mass veto $\rightarrow \mathrm{t\bar{t}} \rightarrow \ell\ell$ dominated: Validate "physics" modeling of $\mathrm{t\bar{t}} \rightarrow \ell\ell$	CR5) $\mathrm{t\bar{t}} \rightarrow \ell\ell$, $\mathrm{t\bar{t}} \rightarrow \ell\tau$ and $\mathrm{t\bar{t}} \rightarrow \ell$fake dominated: Validate τ and fake lepton modeling/ detector effects in $\mathrm{t\bar{t}} \rightarrow \ell\ell$

Table 2: Summary of signal and control regions.

exactly one selected lepton and an isolated track (CR5). The data and MC predicted yields are compared after imposing $E_{\mathrm{T}}^{\mathrm{miss}}$ and M_{T} requirements corresponding to the various signal regions, and the level of agreement is used to assess systematic uncertainties on the $\mathrm{t\bar{t}} \rightarrow \ell\ell$ background. A control region dominated by W+jets is defined by inverting the b-tagging requirement (CR1). A comparison between the data and MC predicted yields after imposing the signal region $E_{\mathrm{T}}^{\mathrm{miss}}$ and M_{T} requirements is used to measure data/MC scale factors and uncertainties, which are applied to the W+jets background. A control region dominated by Z+jets is selected by requiring exactly two leptons with invariant mass consistent with M_Z; this sample is used to compare the impact of jet resolution effects on the large M_{T} tail in data and MC.

6.1 CR4: $\geq$1 b-tag, exactly 2 leptons

The dominant background in our signal regions is $\mathrm{t\bar{t}} \rightarrow \ell\ell$. To verify the contribution of $\mathrm{t\bar{t}} \rightarrow \ell\ell$ to the M_{T} tail in the signal region, we define a control region CR4 by requiring exactly 2 leptons with invariant mass inconsistent with M_Z, and at least 1 b-tagged jet. The MC expected $\mathrm{t\bar{t}} \rightarrow \ell\ell$ purity of this sample is approximately 90%. The M_{T} is constructed using the leading lepton and the $E_{\mathrm{T}}^{\mathrm{miss}}$. Events with a leading electron and those with a leading muon are considered separately and are found to provide consistent results. The $\mathrm{t\bar{t}} \rightarrow \ell\ell$ MC events are first corrected with the K_3 and K_4 scale factors described above, and then normalized to the data in each signal region. The $E_{\mathrm{T}}^{\mathrm{miss}}$ distribution and the M_{T} distribution after a requirement of $E_{\mathrm{T}}^{\mathrm{miss}} > 150$ GeV for data and MC are compared in Figure 3. The $E_{\mathrm{T}}^{\mathrm{miss}}$ and M_{T} requirements corresponding to the signal regions are applied, and the data and MC predicted yields are compared. In general we observe reasonable agreement, although the statistical precision of this test is limited and decreases as the $E_{\mathrm{T}}^{\mathrm{miss}}$ requirement is tightened. Systematic uncertainties on the $\mathrm{t\bar{t}} \rightarrow \ell\ell$ background extracted from this test, and a similar test in events with a lepton and an isolated track (CR5), are discussed in Sec. 6.2.

6.2 CR5: $\geq$ 1 b-tag, 1 lepton + 1 isolated track

Events in CR5 are those that satisfy all selection requirements but fail the isolated track veto. This control region consists of $\mathrm{t\bar{t}} \rightarrow \ell\ell$ (30% purity) and $\mathrm{t\bar{t}} \rightarrow \ell +$ jets where a jet fluctuates to a single high p_{T} isolated track (60% purity). The $\mathrm{t\bar{t}} \rightarrow \ell +$ jets component is significant in the M_{T} peak region, while the events with large M_{T} are dominated by $\mathrm{t\bar{t}} \rightarrow \ell\ell$. As discussed in Sec. 4, the isolated track misidentification rate in $\mathrm{t\bar{t}} \rightarrow \ell +$ jets events is not necessarily well-modeled in MC. Hence the $\mathrm{t\bar{t}} \rightarrow \ell\ell$ background is normalized in the M_{T} peak region before requiring the presence of the isolated track, and the $\mathrm{t\bar{t}} \rightarrow \ell +$ jets background is normalized in the M_{T} peak region after requiring the presence of an isolated track, following the same procedure as is used in the signal region. The distribution of $E_{\mathrm{T}}^{\mathrm{miss}}$ (left) and M_{T} after a requirement of $E_{\mathrm{T}}^{\mathrm{miss}} > 150$

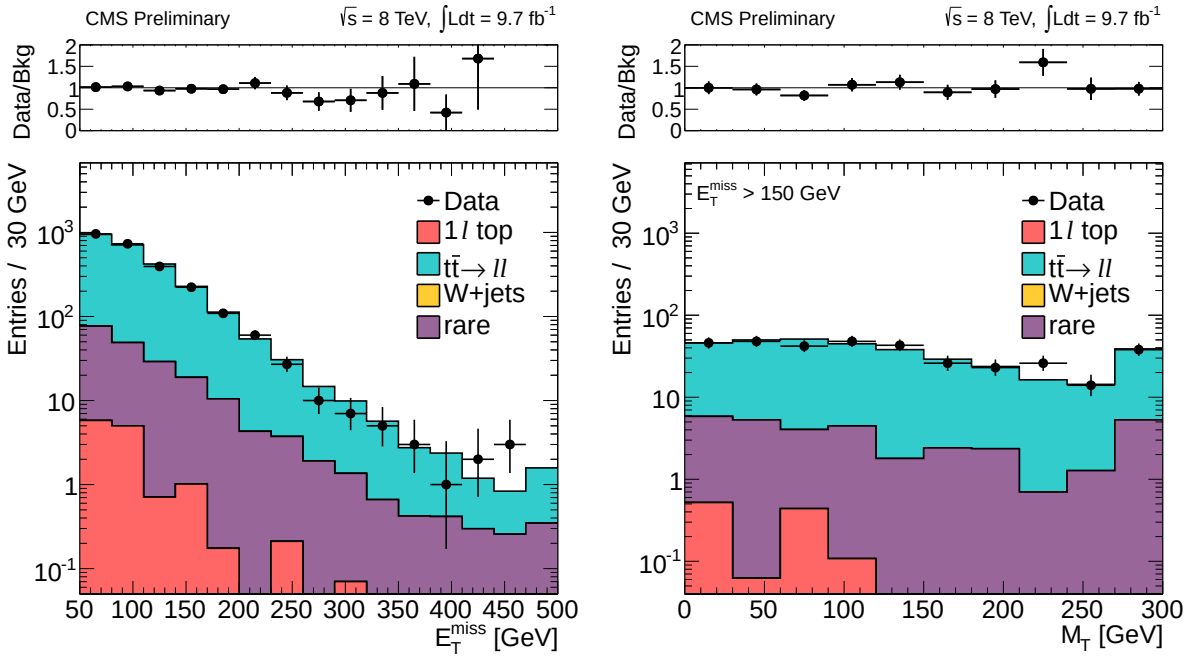

Figure 3: Comparison of the $E_{\mathrm{T}}^{\mathrm{miss}}$ distribution (left) and M_{T} distribution for events satisfying $E_{\mathrm{T}}^{\mathrm{miss}} > 150$ GeV (right) in data vs. MC for CR4.

GeV for both data and MC in CR5 are shown in Figure 4. As in CR4, we apply the $E_{\mathrm{T}}^{\mathrm{miss}}$ and M_{T} requirements for the signal regions and compare the data and MC predicted yields (dominated by $\mathrm{t\bar{t}} \to \ell\ell$), and observe reasonable agreement. The statistical precision of this test is limited due to small event yields, especially in the signal regions defined with tight $E_{\mathrm{T}}^{\mathrm{miss}}$ requirements. We therefore assign systematic uncertainties of 5% (SRA), 10% (SRB), 15% (SRC), 25% (SRD), and 40% (SRE, SRF, SRG). These represent the dominant uncertainties on the $\mathrm{t\bar{t}} \to \ell\ell$ predicted backgrounds in the signal regions. For the $\tilde{t} \to t\chi_1^0$ and $\tilde{t} \to b\chi_1^{\pm} \to b\mathrm{W}\chi_1^0$ decay modes, we have verified that for the model points near the edge of the sensitivity, the contamination of signal events in CR4 and CR5 is significantly smaller than the assessed uncertainty. Since no data/MC scale factors are extracted from these control regions, we do not apply a correction for possible signal contamination.

6.3 CR1: 0 b-tags, exactly 1 lepton

The full event selection is applied to events in this CR, including the isolated track veto, but requiring 0 b-tags. With 0 b-tags and 1 lepton, this region is dominated by W+jets (MC expected purity approximately 75%). It is thus used to extract data/MC corrections for the modeling of this background in the M_{T} tail, and estimate the corresponding uncertainty. Figure 5 shows the $E_{\mathrm{T}}^{\mathrm{miss}}$ distribution and the M_{T} distribution after the requirement $E_{\mathrm{T}}^{\mathrm{miss}} > 150$ GeV, corresponding to SRB. The electron and muon channels are combined, since we observe consistent results in these two channels.

As an initial sanity test, we first check the scale factor needed to match the MC and data in the M_{T} peak region $50 < M_{\mathrm{T}} < 80$ GeV, and verify that it does not deviate significantly from 1. We then compare the observed yields in data and the MC predicted yields after applying $E_{\mathrm{T}}^{\mathrm{miss}}$ and M_{T} requirements corresponding to the signal regions. As shown in Fig. 5 (right), the M_{T} tail in the data is larger than in the MC, and we thus apply data/MC scale factors

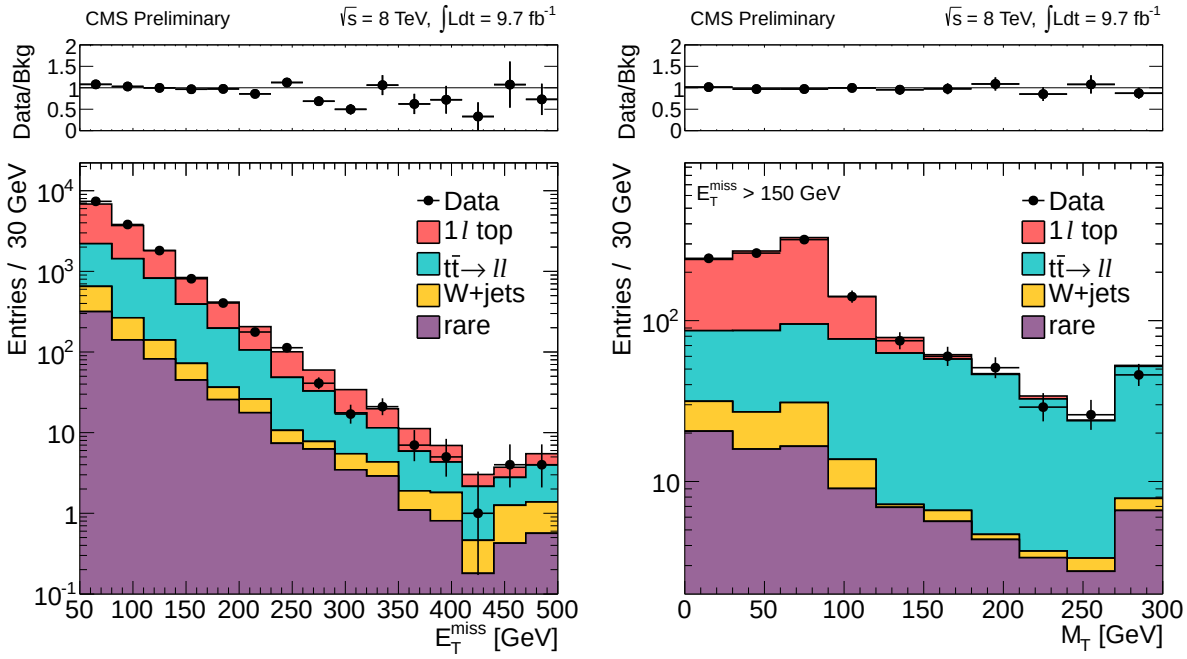

Figure 4: Comparison of the $E_{\mathrm{T}}^{\mathrm{miss}}$ distribution (left) and M_{T} distribution for events satisfying $E_{\mathrm{T}}^{\mathrm{miss}} > 150$ GeV (right) in data vs. MC for CR5.

to the tail-to-peak ratios in the MC. These scale factors are calculated in two ways. First, we compare the total data and total MC predicted yields. Second, we subtract off the non-W+jets backgrounds from the data and compare this to the W+jets MC predicted yields. Since the true scale factor lies somewhere between the two extremes described above, we average these two values. The final scale factors are computed for each SR, and range from 1.0 to 1.6. The uncertainty on these scale factors includes the statistical uncertainty in the data and MC, and half the deviation of the scale factor from 1. The resulting uncertainties vary from (23–100)% for the $E_{\mathrm{T}}^{\mathrm{miss}}$ and M_{T} requirements corresponding to SRA-SRG, reflecting the decrease in the statistical precision of this test as the $E_{\mathrm{T}}^{\mathrm{miss}}$ requirement is increased. Note that while these scale factors deviate significantly from 1 and the corresponding uncertainties are large, the W+jets background makes up only (3–7)% of the total background in the signal regions. As a result, the change in the total background and uncertainty resulting from these correction factors and uncertainties is small compared to the total background uncertainty.

As discussed in Section 4, the tail-to-peak ratio for the single lepton top background is smaller than for the W+jets background, due to the contribution of off-shell W boson production in the W+jets sample. The tail-to-peak ratio of the W+jets sample measured above (R_{W+jets}) thus forms an upper bound for the tail-to-peak ratio of the single lepton top background (R_{top}). A lower bound on R_{top} is formed by taking the value from MC and applying the data/MC scale factor extracted from CR1 as discussed above. Since the true value of R_{top} lies in between these two extremes, we take the average of the upper and lower bounds. The uncertainty includes the statistical uncertainty in the data/MC scale factor from CR1, and half the difference between these upper and lower bounds.

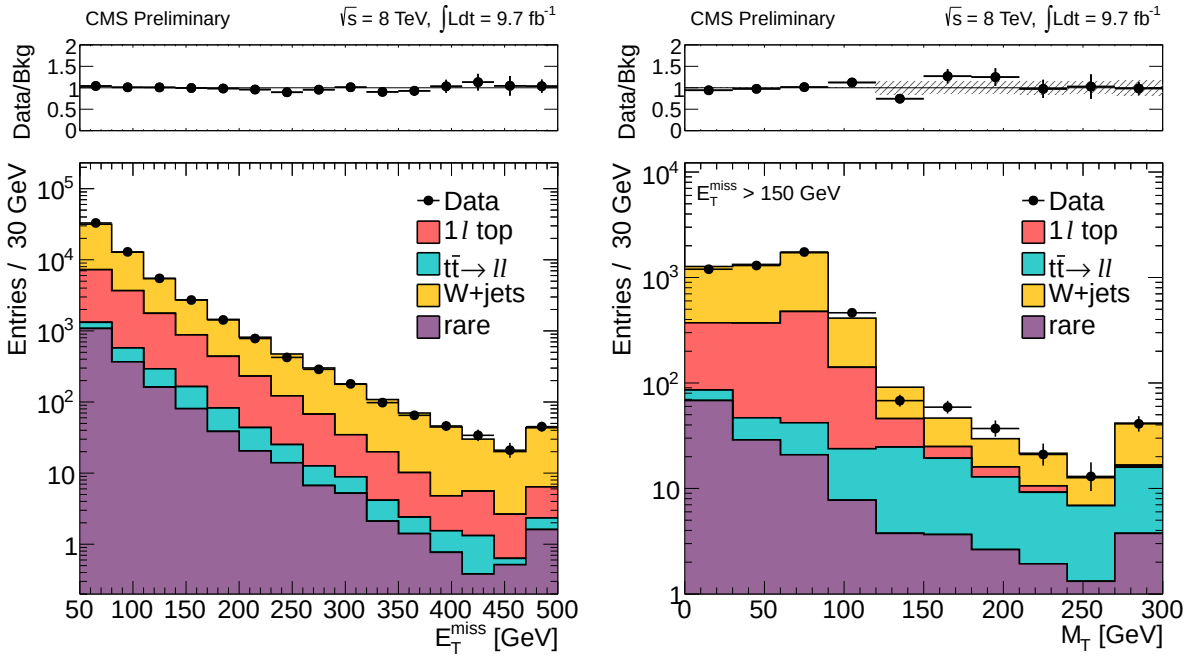

Figure 5: Comparison of the $E_{\mathrm{T}}^{\mathrm{miss}}$ distribution (left) and the M_{T} distribution after a $E_{\mathrm{T}}^{\mathrm{miss}} > 150$ GeV requirement (right) in data vs. MC for events satisfying the requirements of CR1. In the tail of the M_{T} distribution, the data/MC scale factor on the tail-to-peak ratio is applied to the MC. The band corresponds to the uncertainty on the data/MC scale factor.

6.4 CR2: 0 b-tags, exactly 2 leptons

Like CR1, CR2 is designed to test the modeling of the M_{T} tail, but this time it is focused on the single lepton top backgrounds. In single lepton top events, the tail of the M_{T} distribution is dominated by jet resolution effects since the W boson cannot be far off-shell. To test the effect of jet resolution on the tail, we use Z+jets events in data and MC. These events are selected by requiring two good leptons (as described in Section 3) satisfying $81 < M_{\ell\ell} < 101\,\mathrm{GeV}$. Any residual top background is suppressed by requiring 0 b-tags. The MC expected Z+jets purity of this sample is approximately 95%.

To model the $E_{\mathrm{T}}^{\mathrm{miss}}$ we create a "pseudo-$E_{\mathrm{T}}^{\mathrm{miss}}$" by treating the negative lepton as a neutrino and adding it to the measured $E_{\mathrm{T}}^{\mathrm{miss}}$. The M_{T} is then recalculated using this new $E_{\mathrm{T}}^{\mathrm{miss}}$ to create a "pseudo-M_{T}", which is dominated by jet resolution effects, since off-shell Z production fails the $M_{\ell\ell}$ requirement. Figure 6 shows the distribution of pseudo-$E_{\mathrm{T}}^{\mathrm{miss}}$ and pseudo-M_{T} in data vs. MC.

Following a procedure similar to CR1, we compare the data and MC predicted yields for the $E_{\mathrm{T}}^{\mathrm{miss}}$ and M_{T} requirements corresponding to the signal regions. This comparison can in principle be used to extract data/MC scale factors for the tail-to-peak ratios for the single lepton top background, following a procedure similar to the one used in CR1 for the W+jets background. However, the statistical precision of this test is extremely limited, and only allows quantitative results to be extracted for the loosest $E_{\mathrm{T}}^{\mathrm{miss}}$ and M_{T} requirements corresponding to SRA and SRB. For these two regions, this leads to a predicted single lepton top background which is consistent with the nominal prediction following the procedure from Sec. 6.3. Due to the limited statistical precision, we use the results of CR2 only as a cross-check.

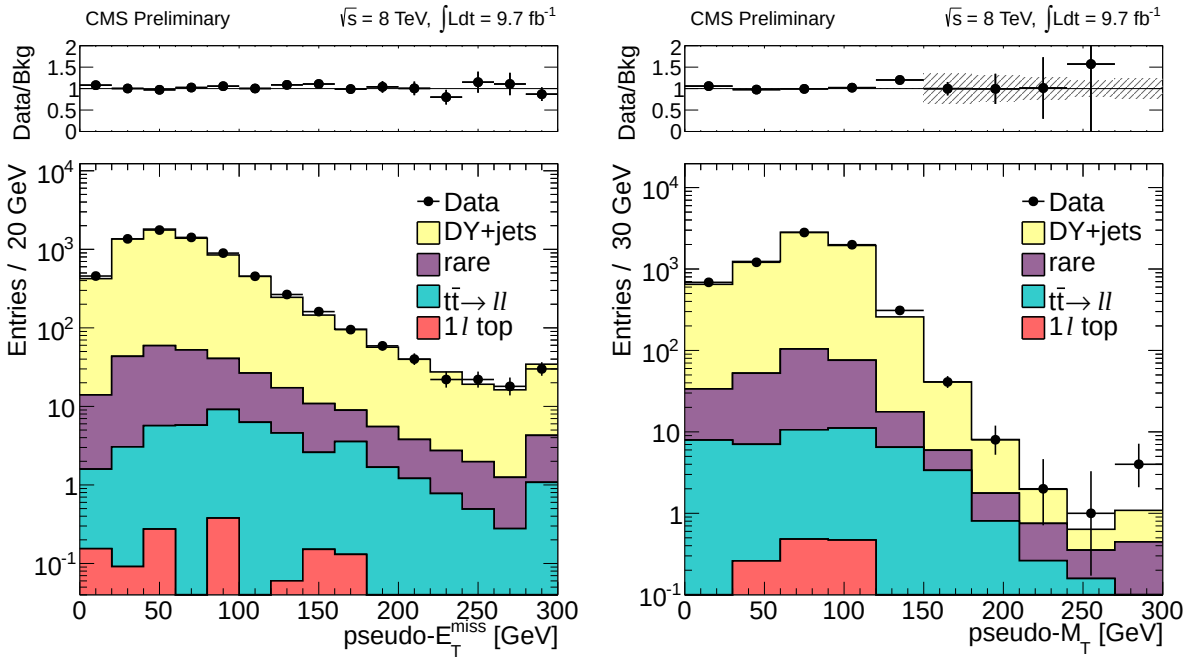

Figure 6: Comparison of the pseudo-$E_{\mathrm{T}}^{\mathrm{miss}}$ distribution (left) and the pseudo-M_{T} distribution (right) in data vs. MC for CR2. In the tail of the pseudo-M_{T} distribution, the data/MC scale factor on the tail-to-peak ratio is applied to the MC. The band corresponds to the uncertainty on the data/MC scale factor.

7 Systematic Uncertainties on the Background Prediction

In this section we summarize the systematic uncertainties on the predicted backgrounds from $t\bar{t} \to \ell\ell$, single lepton top backgrounds, rare, and W+jets backgrounds.

All backgrounds except for the rare contribution are normalized to data in the M_T peak region, so the statistical uncertainties in the data and MC yields in the M_T peak region contribute to the background predictions in the high M_T signal regions. This normalization is repeated after varying the W+jets yield in the M_T peak region by $\pm 50\%$. For the $t\bar{t} \to \ell\ell$ background, the dominant uncertainty is assessed based on the data/MC comparison in the high E_T^{miss} and M_T regions of CR4 and CR5. The statistical uncertainties in the N_{jets} scaling factors K_3 and K_4 also contribute, as well as the uncertainty from limited statistics in the $t\bar{t} \to \ell\ell$ MC sample. There is an additional uncertainty from the efficiency for events with a second lepton (e, μ, or 1-prong hadronic τ decay) within the detector acceptance and satisfying $p_T > 10$ GeV. We verify that the MC reproduces this efficiency by comparing to data in $Z \to \ell\ell$ events, within an uncertainty of 6%. We also verify the stability of the $t\bar{t} \to \ell\ell$ MC background prediction by comparing our nominal POWHEG sample with a sample generated with MADGRAPH, and by varying the generator parameters Q^2 and matching scale up and down by a factor of 2, and varying the top mass from the nominal value of 172.5 GeV up and down to 178.5 and 166.5 GeV. Since the resulting background predictions are consistent within the systematic uncertainties discussed above, we do not assess any additional uncertainty from these tests. The uncertainty in the W+jets and single lepton top backgrounds are dominated by the uncertainty in the peak-to-tail ratios, as determined from data/MC comparisons in CR1. The uncertainty in the rare SM backgrounds is dominated by the 50% uncertainty in the cross section. The systematic uncertainties are summarized in Table 3. In SRA and SRB the dominant uncertainty is from the tail-to-peak ratio for the single lepton top backgrounds. For all other signal regions the uncertainty in the $t\bar{t} \to \ell\ell$ background assessed based on the data to MC comparisons in CR4 and CR5 dominates.

Source	SRA	SRB	SRC	SRD	SRE	SRF	SRG
M_T peak data and MC (stat)	0.9	1.7	2.9	4.7	7.0	10.1	15.4
W+jets cross-section	1.7	2.3	3.0	3.9	4.3	4.3	5.1
K_3 and K_4 N_{jets} scale factors	1.9	2.0	2.1	2.1	2.0	1.9	1.8
$t\bar{t} \to \ell\ell$ (CR4 and CR5 tests)	3.1	6.5	10.3	17.3	26.1	24.7	24.5
2nd lepton veto	1.2	1.3	1.4	1.4	1.3	1.2	1.2
$t\bar{t} \to \ell\ell$ (stat)	1.2	1.6	3.0	5.1	7.4	11.1	13.6
top tail-to-peak ratio	12.5	8.7	8.5	6.5	7.7	9.5	6.0
W+jets tail-to-peak ratio	6.4	5.2	5.7	6.6	9.6	13.3	17.6
rare cross-sections	2.0	2.2	3.2	4.9	6.4	6.2	7.6
total	14.9	12.9	15.9	21.8	31.7	34.2	38.2

Table 3: Summary of the contributions to the relative uncertainties in the background predictions, and the total relative background uncertainty. All values are quoted in %.

8 Results

A summary of the background expectations after applying all the corrections and the corresponding data counts are shown in Table 4 for each of the signal regions, for the electron channel, muon channel, and the sum of these two channels. The observed yields in the signal regions are in good agreement with the predicted background. No evidence for an excess is observed. The predicted and observed E_T^{miss} distributions for events satisfying the signal

region requirement $M_{\mathrm{T}} > 120$ GeV are displayed in Fig. 7. Data to MC comparisons of the M_{T} distribution with $E_{\mathrm{T}}^{\mathrm{miss}}$ requirements corresponding to SRA and SRB are displayed in Fig. 8. The interpretation of these results in the context of models of top squark pair production is presented in Section 9.

Sample	SRA	SRB	SRC	SRD	SRE	SRF	SRG
Muon							
$\mathrm{t\bar{t}} \to \ell\ell$	331 ± 22	183 ± 21	59.5 ± 10.0	23 ± 6	9.0 ± 3.9	3.7 ± 1.8	2.2 ± 1.2
$\mathrm{t\bar{t}} \to \ell +$ jets & single top (1ℓ)	148 ± 75	67.9 ± 28.9	16.1 ± 9.1	4.7 ± 3.2	1.8 ± 1.6	0.9 ± 0.9	0.4 ± 0.5
W+jets	19.2 ± 4.5	10.0 ± 2.2	3.11 ± 0.98	1.2 ± 0.6	0.6 ± 0.4	0.4 ± 0.3	0.2 ± 0.2
Rare	33.2 ± 16.6	22.7 ± 11.4	9.00 ± 4.50	4.8 ± 2.4	2.9 ± 1.5	1.2 ± 0.6	1.0 ± 0.5
Total	531 ± 80	284 ± 37	87.7 ± 14.2	33 ± 7	14 ± 5	6.1 ± 2.1	3.8 ± 1.4
Data	494	254	76	31	8	2	1
Electron							
$\mathrm{t\bar{t}} \to \ell\ell$	248 ± 17	144 ± 17	51.1 ± 8.8	16 ± 5	5.5 ± 2.5	2.5 ± 1.3	1.3 ± 0.7
$\mathrm{t\bar{t}} \to \ell +$ jets & single top (1ℓ)	108 ± 55	51.8 ± 22.1	12.9 ± 7.3	3.0 ± 2.0	1.2 ± 1.1	0.7 ± 0.7	0.4 ± 0.5
W+jets	14.3 ± 3.3	7.50 ± 1.66	2.43 ± 0.77	0.8 ± 0.4	0.4 ± 0.3	0.3 ± 0.2	0.1 ± 0.2
Rare	25.8 ± 12.9	15.8 ± 7.9	7.10 ± 3.55	2.9 ± 1.5	0.7 ± 0.4	0.3 ± 0.2	0.1 ± 0.1
Total	396 ± 59	219 ± 29	73.5 ± 11.9	23 ± 5	7.8 ± 2.7	3.9 ± 1.5	1.9 ± 0.9
Data	367	202	74	30	15	7	2
Muon+Electron Combined							
$\mathrm{t\bar{t}} \to \ell\ell$	579 ± 38	328 ± 37	111 ± 18	39 ± 10	14 ± 6	6.2 ± 2.9	3.5 ± 1.8
$\mathrm{t\bar{t}} \to \ell +$ jets & single top (1ℓ)	256 ± 131	120 ± 51	29.0 ± 16.4	7.7 ± 5.1	3.1 ± 2.7	1.7 ± 1.6	0.8 ± 1.0
W+jets	33.5 ± 8.2	17.5 ± 4.5	5.54 ± 1.98	2.0 ± 1.0	1.0 ± 0.7	0.7 ± 0.6	0.3 ± 0.4
Rare	59.0 ± 29.5	38.5 ± 19.3	16.1 ± 8.1	7.7 ± 3.9	3.6 ± 1.8	1.5 ± 0.8	1.1 ± 0.6
Total	927 ± 138	504 ± 65	161 ± 26	56 ± 12	22 ± 7	10 ± 3	5.7 ± 2.2
Data	861	456	150	61	23	9	3

Table 4: The result of the search. For each signal region the individual background contributions, total background, and observed yields are indicated. The uncertainty includes both the statistical and systematic components.

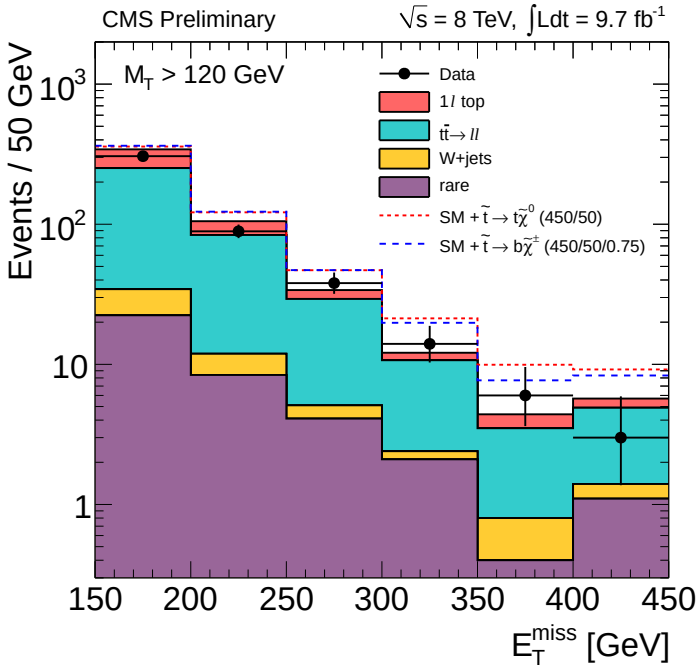

Figure 7: Comparison of the $E_{\mathrm{T}}^{\mathrm{miss}}$ distributions in data vs. predicted background, after the signal region requirement $M_{\mathrm{T}} > 120$ GeV. Expected $E_{\mathrm{T}}^{\mathrm{miss}}$ distributions from two sample signal points are indicated: $\tilde{t} \to t\tilde{\chi}_1^0$ where $m_{\tilde{t}} = 450$ and $m_{\tilde{\chi}_1^0} = 50$ GeV, and $\tilde{t} \to b\tilde{\chi}_1^{\pm} \to b\mathrm{W}^{\pm}\tilde{\chi}_1^0$ where $m_{\tilde{t}} = 450$, $m_{\tilde{\chi}_1^{\pm}} = x m_{\tilde{t}} + (1-x) m_{\tilde{\chi}_1^0}$ with $x = 0.75$ and $m_{\tilde{\chi}_1^0} = 50$ GeV.

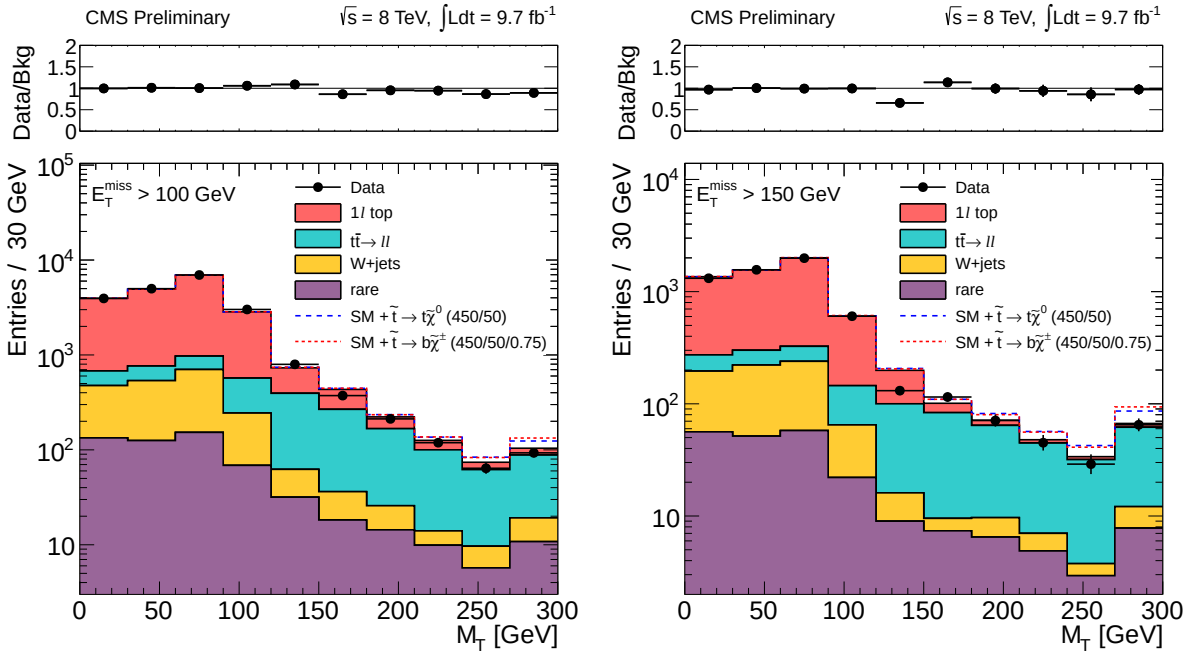

Figure 8: Comparison of the M_{T} distributions in data vs. MC for events with $E_{\mathrm{T}}^{\mathrm{miss}} > 100$ GeV (left, corresponding to SRA) and $E_{\mathrm{T}}^{\mathrm{miss}} > 150$ GeV (right, corresponding to SRB). Expected M_{T} distributions from two sample signal points are indicated: $\tilde{t} \to t\tilde{\chi}_1^0$ where $m_{\tilde{t}} = 450$ and $m_{\tilde{\chi}_1^0} = 50$ GeV, and $\tilde{t} \to b\tilde{\chi}_1^{\pm} \to b\mathrm{W}^{\pm}\tilde{\chi}_1^0$ where $m_{\tilde{t}} = 450$, $m_{\tilde{\chi}_1^{\pm}} = x m_{\tilde{t}} + (1-x) m_{\tilde{\chi}_1^0}$ with $x = 0.75$ and $m_{\tilde{\chi}_1^0} = 50$ GeV.

9 Interpretation

In this section the results of Table 4 are interpreted in the context of simplified models of top squark pair production [27–29]. Signal events are normalized to NLO+NLL cross sections, and we consider theoretical uncertainties including renormalization and factorization scale, parton density functions (PDFs), and the strong coupling strength α_S [30].

The $\tilde{t}$ decay matrix element is treated as flat, which is equivalent to the assumption of 50/50 mixing of left-handed and right-handed top superpartners. Two decay modes are considered, $\tilde{t} \to t\tilde{\chi}_1^0$ and $\tilde{t} \to b\tilde{\chi}_1^\pm \to b\mathrm{W}\tilde{\chi}_1^0$. In both scenarios, we present cross section limits and exclude a region of the $m_{\tilde{t}}$ vs. $m_{\tilde{\chi}_1^0}$ parameter space. For the $\tilde{t} \to b\tilde{\chi}_1^\pm$ scenario the mass of the intermediate $\tilde{\chi}_1^\pm$ is specified by the parameter x, defined as $m_{\tilde{\chi}_1^\pm} = x m_{\tilde{t}} + (1-x) m_{\tilde{\chi}_1^0}$. We consider two cases: $x = 0.75$ (the $\tilde{\chi}_1^\pm$ is closer in mass to the $\tilde{t}$), and $x = 0.5$ (the $\tilde{\chi}_1^\pm$ mass is half-way between the $\tilde{t}$ and $\tilde{\chi}_1^0$ masses). Our analysis is not sensitive to the $x = 0.25$ scenario.

We consider the following several sources of systematic uncertainty in the signal acceptance and efficiency. The uncertainty in the integrated luminosity is 4.4%. The trigger efficiency for events with a selected lepton is measured using samples of $\mathrm{Z} \to \ell\ell$, with an uncertainty of 3%. The simulated events reproduce the lepton identification and isolation efficiencies measured in data using samples of $\mathrm{Z} \to \ell\ell$ within 2%. To account for small differences in the b-tagging efficiencies measured in data and simulation, a scale factor of $(98 \pm 2)\%$ is applied to simulated events. The uncertainty from the jet and $E_\mathrm{T}^\mathrm{miss}$ energy scale is determined separately for each point in the signal model parameter space. The jet transverse energies are varied by their uncertainties and used to determine the uncertainty in the selection efficiency for the jet multiplicity, $E_\mathrm{T}^\mathrm{miss}$, and M_T requirements. For the loosest signal region SRA this uncertainty varies across the model parameter space in the range (2–15)%. For the tightest signal region SRG the uncertainty varies in the range (4–30)%. This uncertainty is largest when the differences between the masses of the top squark and LSP are small.

Next, upper limits on the signal cross section are calculated separately for each signal region, incorporating the uncertainties in the signal acceptance and efficiency discussed above, using the LHC-type CLs criterion. For each point in the signal model parameter space, the observed limit is taken from the signal region with the best expected limit. The most sensitive signal regions for each of the top squark decay modes are presented in Appendix A. The results are displayed in Fig. 9 ($\tilde{t} \to t\tilde{\chi}_1^0$) and Fig. 10 ($\tilde{t} \to b\tilde{\chi}_1^\pm$, $\tilde{\chi}_1^\pm \to \mathrm{W}\tilde{\chi}_1^0$). For the $\tilde{t} \to t\tilde{\chi}_1^0$ scenario, these results probe top squarks with masses in the range of approximately 230–430 GeV, for neutralino masses less than approximately 110 GeV. For the $\tilde{t} \to b\tilde{\chi}_1^\pm$ scenario with $x = 0.75$, these results probe top squarks with masses in the range of approximately 160–420 GeV, for neutralino masses less than approximately 120 GeV. The sensitivity is reduced in the $x = 0.5$ scenario, where the results probe top squarks with masses in the range of approximately 260–340 GeV, for neutralino masses less than approximately 80 GeV.

A search by the ATLAS collaboration obtained similar sensitivity for the $\tilde{t} \to t\tilde{\chi}_1^0$ scenario with a data sample of 7 TeV pp collisions corresponding to an integrated luminosity of approximately 5 fb^{-1} [8]. The most important difference between the two analyses is the requirement of hadronic top mass reconstruction in the ATLAS selection. This requirement significantly reduces the $\mathrm{t\bar{t}} \to \ell\ell$ background; however, it is not used in our search to maintain efficiency for the $\tilde{t} \to b\tilde{\chi}_1^\pm$ decay mode. Furthermore, the ATLAS model assumes large right-handed polarization, while we take the top quark in the $\tilde{t} \to t\tilde{\chi}_1^0$ decay to be unpolarized, resulting in a lower signal selection efficiency in our analysis.

10 Summary

This note presents a search for the direct pair production of top squarks, in the final state consisting of a single isolated lepton, jets, and large transverse mass. Good agreement is observed between the observed yields and the predicted backgrounds in several signal regions, defined by requirements of large $E_{\mathrm{T}}^{\mathrm{miss}}$ and M_{T}. The results are interpreted in the context of simplified models of top squark pair production, and probe top squarks with masses in the range 160–430 GeV.

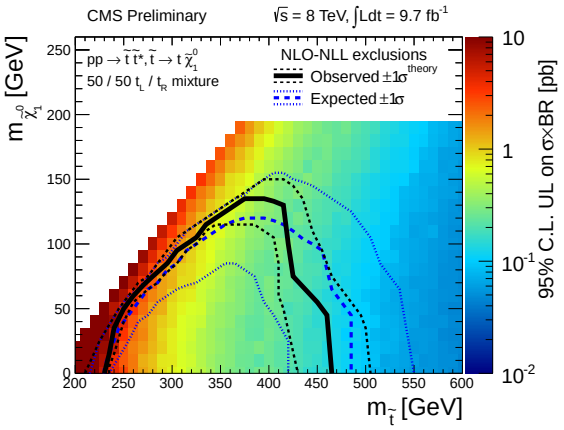

Figure 9: Interpretation in the top squark pair production model with $\tilde{t} \to t\tilde{\chi}_1^0$, in the plane of $m_{\tilde{\chi}_1^0}$ vs. $m_{\tilde{t}}$. The shading indicates the upper limit on the signal cross section. The observed, median expected, and $\pm 1\sigma$ expected exclusion contours are indicated assuming NLO-NLL cross sections, as well as the observed contours when the theory cross section is varied by $\pm 1\sigma$ (the region below the contours is excluded).

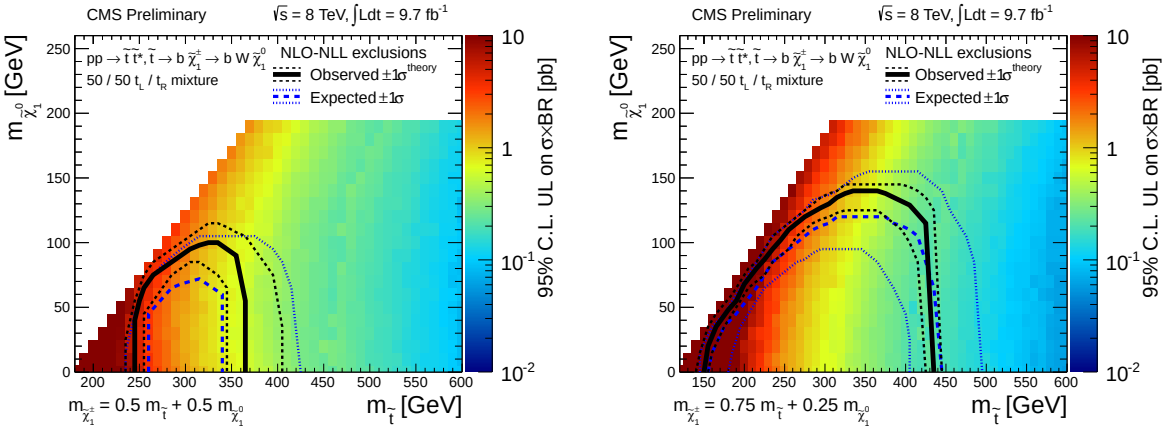

Figure 10: Interpretation in the top squark pair production model with $\tilde{t} \to b\tilde{\chi}_1^{\pm} \to bW\tilde{\chi}_1^0$, in the plane of $m_{\tilde{\chi}_1^0}$ vs. $m_{\tilde{t}}$, for the chargino mass parameter $x = 0.5$ (left) and $x = 0.75$ (right). Details are the same as in Fig. 9.

References

[1] R. Barbieri and G. Giudice, "Upper Bounds on Supersymmetric Particle Masses", *Nucl. Phys.* **B306** (1988) 63, doi:10.1016/0550-3213(88)90171-X.

[2] B. de Carlos and J. Casas, "One-loop analysis of the electroweak breaking in supersymmetric models and the fine-tuning problem", *Phys. Lett.* **B309** (1993), no. 34, 320, doi:10.1016/0370-2693(93)90940-J.

[3] S. Dimopoulos and G. Giudice, "Naturalness constraints in supersymmetric theories with non-universal soft terms", *Phys. Lett.* **B357** (1995), no. 4, 573, doi:10.1016/0370-2693(95)00961-J.

[4] R. Barbieri, G. Dvali, and L. J. Hall, "Predictions from a U(2) flavour symmetry in supersymmetric theories", *Phys. Lett.* **B377** (1996), no. 13, 76, doi:10.1016/0370-2693(96)00318-8.

[5] M. Papucci, J. T. Ruderman, and A. Weiler, "Natural SUSY Endures", *J. HEP* **1209** (2012) 035, doi:10.1007/JHEP09(2012)035, arXiv:1110.6926.

[6] M. W. Cahill-Rowley, J. L. Hewett, A. Ismail et al., "The Higgs Sector and Fine-Tuning in the pMSSM", *Phys. Rev.* **D86** (2012) 075015, doi:10.1103/PhysRevD.86.075015, arXiv:1206.5800.

[7] ATLAS Collaboration, "Search for a supersymmetric partner to the top quark in final states with jets and missing transverse momentum at $\sqrt{s}$ = 7 TeV with the ATLAS detector", arXiv:1208.1447. Submitted to *Phys. Rev. Lett.*

[8] ATLAS Collaboration, "Search for direct top squark pair production in final states with one isolated lepton, jets, and missing transverse momentum in $\sqrt{s}$ = 7 TeV pp collisions using 4.7 fb-1 of ATLAS data", arXiv:1208.2590. Submitted to *Phys. Rev. Lett.*

[9] ATLAS Collaboration, "Search for light scalar top quark pair production in final states with two leptons with the ATLAS detector in $\sqrt{s}$ = 7 TeV proton-proton collisions", arXiv:1208.4305. Submitted to *Eur. Phys. J C*.

[10] ATLAS Collaboration, "Search for light top squark pair production in final states with leptons and b-jets with the ATLAS detector in $\sqrt{s}$ = 7 TeV proton-proton collisions", arXiv:1209.2102. Submitted to *Phys. Lett. B*.

[11] ATLAS Collaboration, "Search for a heavy top-quark partner in final states with two leptons with the ATLAS detector at the LHC", arXiv:1209.4186. Submitted to *J. HEP*.

[12] CDF Collaboration, "Search for the supersymmetric partner of the top quark in $p\bar{p}$ collisions at $\sqrt{s}$ = 1.96 TeV", *Phys. Rev.* **D82** (2010) 092001, doi:10.1103/PhysRevD.82.092001, arXiv:1009.0266.

[13] D0 Collaboration, "Search for pair production of the scalar top quark in the electron+muon final state", *Phys. Lett.* **B696** (2011) 321, doi:10.1016/j.physletb.2010.12.052, arXiv:1009.5950.

[14] CMS Collaboration, "The CMS experiment at the CERN LHC", *J. Inst* **3** (2008) S08004, doi:10.1088/1748-0221/3/08/S08004.

[15] CMS Collaboration, "Performance of muon identification in pp collisions at $\sqrt{s}$ = 7 TeV", CMS Physics Analysis Summary CMS-PAS-MUO-10-002, (2010).

[16] CMS Collaboration, "Electron Reconstruction and Identification at $\sqrt{s} = 7$ TeV", CMS Physics Analysis Summary CMS-PAS-EGM-10-004, (2010).

[17] CMS Collaboration, "Commissioning of the Particle-Flow Reconstruction in Minimum-Bias and Jet Events from pp Collisions at 7 TeV", CMS Physics Analysis Summary CMS-PAS-PFT-10-002, (2010).

[18] M. Cacciari, G. P. Salam, and G. Soyez, "The anti-k_t jet clustering algorithm", *J. HEP* **04** (2008) 063, doi:10.1088/1126-6708/2008/04/063, arXiv:0802.1189.

[19] CMS Collaboration, "b-Jet Identification in the CMS Experiment", CMS Physics Analysis Summary CMS-PAS-BTV-11-004, (2012).

[20] T. Sjöstrand, S. Mrenna, and P. Z. Skands, "PYTHIA 6.4 Physics and Manual", *J. HEP* **05** (2006) 026, doi:10.1088/1126-6708/2006/05/026, arXiv:hep-ph/0603175.

[21] J. Alwall, "MadGraph/MadEvent v4: the new web generation", *J. HEP* **09** (2007) 028, doi:10.1088/1126-6708/2007/09/028.

[22] S. Frixione, P. Nason, and C. Oleari, "Matching NLO QCD computations with parton shower simulations: the POWHEG method", *J. HEP* **11** (2007) 070, doi:10.1088/1126-6708/2007/11/070, arXiv:0709.2092.

[23] P. M. Nadolsky, H.-L. Lai, Q.-H. Cao et al., "Implications of CTEQ global analysis for collider observables", *Phys. Rev. D* **78** (2008) 013004, doi:10.1103/PhysRevD.78.013004, arXiv:0802.0007.

[24] M. Kramer, A. Kulesza, R. van der Leeuw et al., "Supersymmetry production cross sections in pp collisions at $\sqrt{s}$ = 7 TeV", arXiv:1206.2892.

[25] GEANT4 Collaboration, "GEANT4–a simulation toolkit", *Nucl. Instrum. Meth. A* **506** (2003) 250, doi:10.1016/S0168-9002(03)01368-8.

[26] CMS Collaboration, "The fast simulation of the CMS detector at LHC", *J. Phys. Conf. Ser.* **331** (2011) 032049, doi:10.1088/1742-6596/331/3/032049.

[27] LHC New Physics Working Group Collaboration, "Simplified Models for LHC New Physics Searches", *J. Phys.* **G39** (2012) 105005, doi:10.1088/0954-3899/39/10/105005, arXiv:1105.2838.

[28] N. Arkani-Hamed et al., "MARMOSET: The Path from LHC Data to the New Standard Model via On-Shell Effective Theories", (2007). arXiv:hep-ph/0703088.

[29] B. Knuteson and S. Mrenna, "BARD: Interpreting New Frontier Energy Collider Physics", (2006). arXiv:hep-ph/0602101.

[30] M. Botje et al., "The PDF4LHC Working Group Interim Recommendations", (2011). arXiv:1101.0538.

A Most Sensitive Signal Regions

In this appendix, the most sensitive signal regions for each of the top squark decay modes are presented in the model parameter space of $m_{\tilde{\chi}_1^0}$ vs. $m_{\tilde{t}}$, for the $\tilde{t} \to t\tilde{\chi}_1^0$ scenario (Fig. 11) and $\tilde{t} \to b\tilde{\chi}_1^{\pm}$ scenario (Fig. 12 and 13).

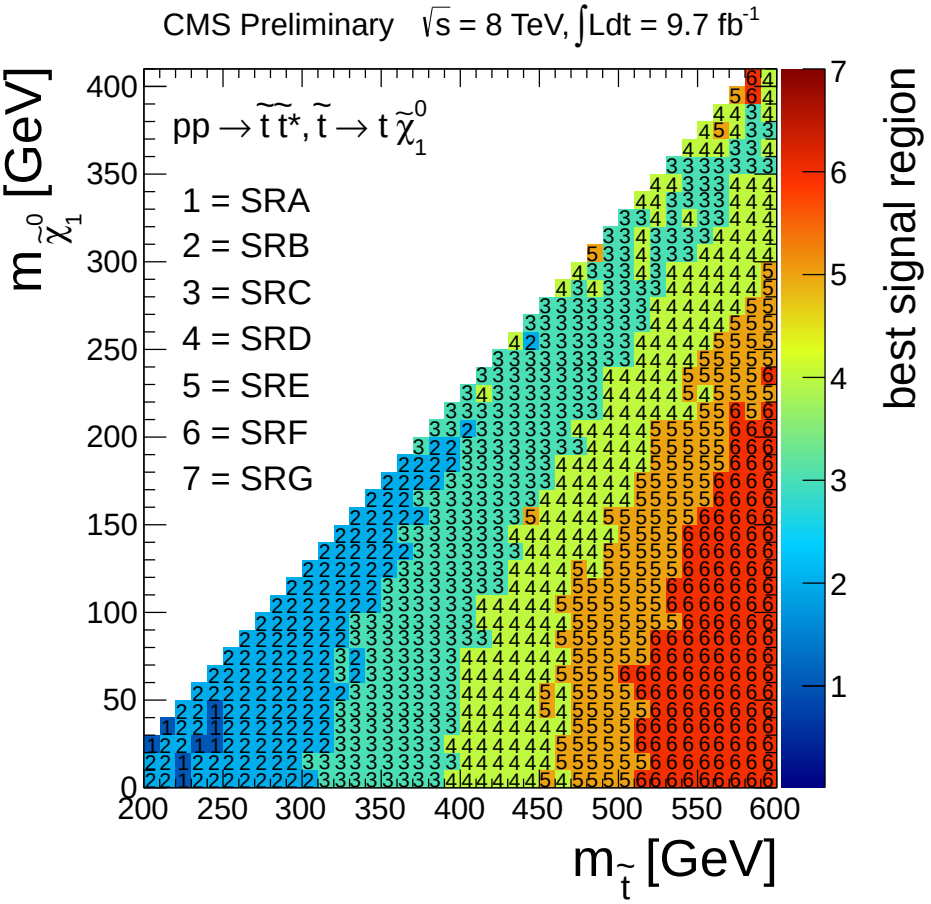

Figure 11: The signal region with the best sensitivity for the $\tilde{t} \to t\tilde{\chi}_1^0$ decay, in the plane of $m_{\tilde{\chi}_1^0}$ vs. $m_{\tilde{t}}$.

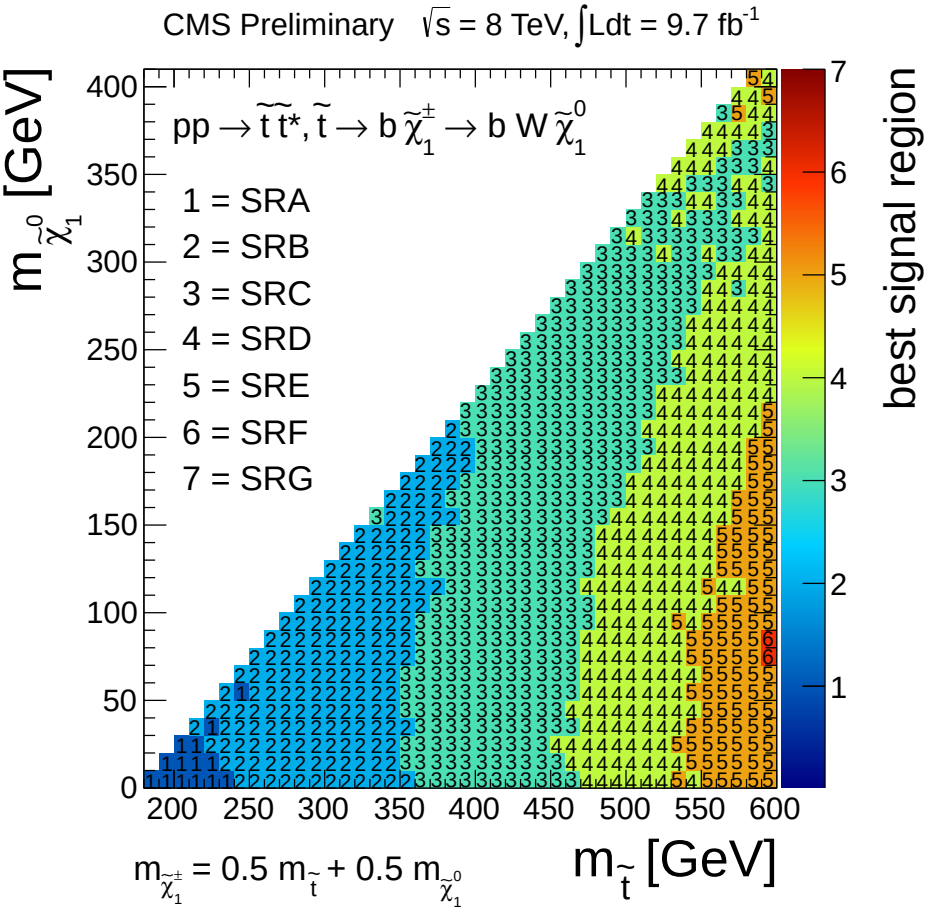

Figure 12: The signal region with the best sensitivity for the $\tilde{t} \to b\tilde{\chi}_1^{\pm}$ decay for $x = 0.5$, in the plane of $m_{\tilde{\chi}_1^0}$ vs. $m_{\tilde{t}}$.

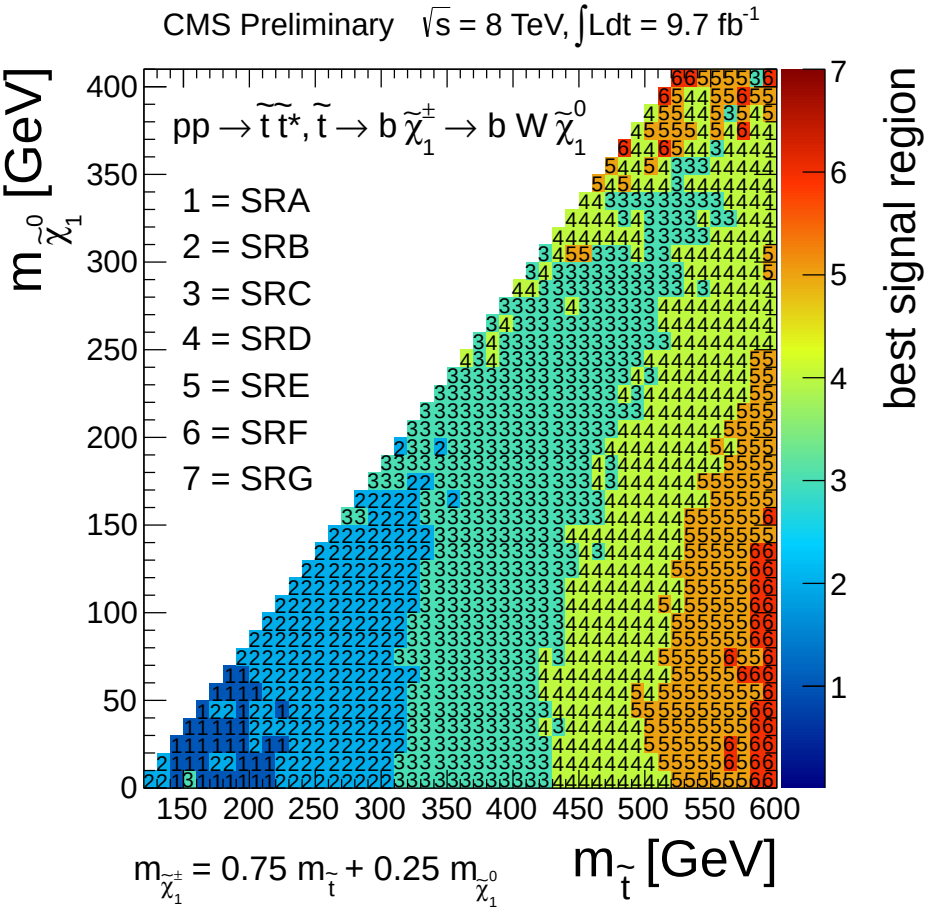

Figure 13: The signal region with the best sensitivity for the $\tilde{t} \to b\tilde{\chi}_1^{\pm}$ decay for $x = 0.75$, in the plane of $m_{\tilde{\chi}_1^0}$ vs. $m_{\tilde{t}}$.